Identification and characterization of a wet adhesive protein extracted from *Dreissena bugensis*, the freshwater quagga mussel

Angelico R. Obille[1], Rida Hasan[1], David J. Rees[1], Judith Ng[1], Karina M. M. Carneiro[1,2], Eli D. Sone*[1,2,3]

[1] Institute of Biomedical Engineering, University of Toronto, Toronto, ON, Canada, M5S 3G9
[2] Faculty of Dentistry, University of Toronto, Toronto, ON, Canada, M5G 1G6
[3] Department of Materials Science & Engineering, University of Toronto, Toronto, ON, Canada, M5S 3E4

* **Corresponding author**: Eli D. Sone (eli.sone@utoronto.ca; 416-978-7422; 124 Edward Street, Toronto, ON, Canada, M5G 1G6)

Classification: Biological Sciences/Biochemistry
Keywords: quagga mussels, byssus, mussel adhesive protein, freshwater bioadhesion, atomic force microscopy

Abstract

Mechanisms of wet adhesion have been developed by several aquatic organisms over millions of years of evolutionary processes. Yet, the repertoire of synthetic biocompatible wet adhesive materials is still limited. In most marine bioadhesive proteins, 3,4-dihydroxyphenylalanine (DOPA) plays a significant role in strong interfacial interactions. The bioadhesive proteins in freshwater organisms are less well understood. The quagga mussel (*Dreissena bugensis*) is a notorious freshwater invasive species in the Great Lakes that attaches to a plethora of surfaces via a byssus. To determine the adhesive proteins in the quagga mussel byssus, we utilized quantitative proteomics to identify the proteins enriched at the byssus-substrate interface. Among the identified proteins was the Dbfp7 protein family. Dbfp7 is a small, polymorphic, and mostly disordered protein that lacks significant amounts of DOPA. Atomic force microscopy measurements of Dbfp7 confirm that this protein has similar adhesion energy to marine mussel adhesive proteins in aqueous conditions despite lacking DOPA. These results suggest that freshwater mussels may employ different mechanisms of adhesion compared to marine byssates. The inclusion of Dbfp7 to the library of known wet bioadhesive proteins – the first functionally characterized freshwater bioadhesive protein to our knowledge – will allow for a better understanding of the fundamental properties required to achieve biocompatible wet adhesion, a crucial step for the development of bio-inspired wet adhesive materials, such as improved medical adhesives.

Significance Statement

While many aquatic organisms evolved strategies to adhere to surfaces underwater, current synthetic biocompatible adhesives lack reliable adhesive strength in varying aqueous conditions. Investigating freshwater mussel adhesive proteins expands the current understanding of aquatic bioadhesion and offers potential advancements in wet adhesive technology. The discovery of a DOPA-deficient wet adhesive protein derived from the invasive quagga mussels presents a paradigm shift to the currently known mechanisms of byssal bioadhesion, thereby expanding the repertoire of wet adhesive strategies. Further, understanding the mechanism of adhesion employed by this biofouling species can help with the design of anti-fouling strategies to mitigate the impacts of these animals on the infrastructure and ecosystems in the Great Lakes and connected freshwater systems in North America.

Introduction

Adhesives found in nature perform in ways that synthetic adhesives have yet to match. For example, even though many aquatic organisms have adapted to adhere to surfaces underwater, it remains an engineering challenge to synthesize strong, biocompatible adhesives that are effective in wet conditions. One strategy that has been developed in nature over millions of years of natural selection is adherence via a structure called the byssus. The byssus is utilized by several bivalves, including marine mussels, oysters, and a few freshwater mussels, to permanently attach themselves and support their sessile lifestyle (1). The byssus is composed of individual proteinaceous threads extending from the body of the animal, with each thread ending distally in a flattened plaque. The bulk of the plaque material connects the thread to the adhesive proteins found at the plaque-substrate interface. These interfacial proteins bind so strongly that when plaques are detached, a residue called the footprint usually remains (2–5).

Originating from the Dnieper River in Eastern Europe and found more recently in the Great Lakes basin and connected waterways in North America, quagga mussels (*Dreissena bugensis*) and zebra mussels (*Dreissena polymorpha*) are invasive species that are among only a handful of freshwater byssates (6). Although superficially similar to that of the well-studied marine byssates, the biochemical composition of the *Dreissenid* byssus is unique; *Mytilid* byssal proteins and *Dreissenid* byssal proteins share very little homology (7, 8). Moreover, amounts of peptidyl 3,4-dihydroxyphenylalanine (DOPA) in *Dreissenid* byssal proteins are considerably lower than in marine mussels and are distributed evenly between the byssal thread and plaque rather than concentrated in the plaque (9). This suggests that in the context of protein-substrate interactions, *Dreissenids* may have evolved to employ a unique mechanism of adhesion that relies less heavily on DOPA-based interfacial interactions than their marine counterparts.

Byssal adhesive proteins that have been characterized in the current literature are predominantly in the marine context, i.e. in ocean environments with high ionic composition (1). The best studied system is the byssus of marine mussels of the genus *Mytilus* (10–14). Following the discovery of the significant role of DOPA in interfacial

adhesion in marine mussels and other marine bioadhesive systems, DOPA-based adhesion has been established as a central paradigm for solutions to the problem of biocompatible wet adhesion (15–18). Subsequently, several materials utilizing DOPA-based chemistry for adhesion and cross-linking have been developed (19–24, 13, 25–29). Few of these materials, however, have translated to the clinical setting for medical adhesives, in part due to the propensity for catechol to oxidize into the non-adhesive DOPA-quinone form when exposed to pH values higher than 6.8 (30–32, 25). Aside from translational considerations, the direct effect of ionic strength in the adhesive mechanism of DOPA-based bioadhesion is still unclear (33–35). Studying bioadhesives from freshwater systems can help expand the current repertoire of biocompatible wet adhesives.

Sequencing of the quagga mussel foot transcriptome combined with bottom-up proteomics led to the determination of fourteen novel *Dreissena bugensis* foot protein sequences (Dbfp4 to Dbfp17), and more complete sequences of known Dbfp1 and Dbfp2 (8, 9, 36). The location and function of each protein, however, remains elusive. Of particular interest are the proteins at the plaque-substrate interface, where a 10 to 20 nm thick electron-dense footprint protein layer is present, as observed by transmission electron microscopy (TEM) (2). Here, we report the relative enrichment of the proteins in the bulk plaque and footprint via quantitative proteomics. This method allowed us to identify the proteins significantly enriched in the footprint, signifying potential adhesive ability. Among this set of footprint proteins is Dbfp7, a family of proteins that: matches the molecular weights of proteins detected by matrix-assisted laser desorption/ionization time-of-flight (MALDI-TOF) mass spectrometry (37), has been shown to be a significant portion of the byssus (8), and herein is shown to be adhesive in aqueous conditions despite lacking DOPA.

Results

Quantitative liquid chromatography tandem mass spectrometry (LC-MS/MS) was used to identify the byssal proteins that are relatively more abundant in the footprint compared to the bulk plaque extracts. Quagga mussels collected from Lake Ontario were allowed to lay fresh byssi onto glass slides overnight. Footprint (FP) and bulk plaque (BP) proteins were separately solubilized in extraction buffer following scraping of the bulk plaque, which leaves behind a “footprint” residue on the slide (**Figure 1A**) (3–5, 8, 9). The footprint and bulk plaque solubilized proteins were digested with trypsin and the peptides were subsequently functionalized with tandem mass tag (TMT) labels. The tagged peptides were pooled then sequenced via LC-MS/MS (**Figure 1B**). The peptide sequences were fingerprinted against the quagga mussel foot transcriptome (8), searched against protein databases using the basic local alignment search tool (BLAST) algorithm for homology assessment and identification of proteins, and compared to proteins identified from whole-thread/plaque byssal material that was induced to be secreted by potassium chloride (KCl) injection in the pedal ganglion (IND); the induced byssus dataset has been previously reported (8).

Identification of plaque proteins in the naturally secreted quagga mussel byssus

The induced byssus includes proteins composing the entire byssus, i.e. thread proteins, bulk plaque proteins, and footprint proteins. In the naturally secreted samples, bulk plaque and footprint samples were collected in separate groups, and the threads were discarded. The plaque protein collection method cannot precisely separate the bulk plaque from the footprint material. As a result, footprint proteins are expected to be present in the bulk plaque group (albeit to a lesser extent) and vice versa. For this reason, the ‘Footprint + Bulk Plaque’ group and the ‘ALL’ group were considered to most reliably contain proteins localized to the plaque (**Figure 1D**). These proteins were identified by the BLASTp algorithm and include (full list in **Table S1**): Dbfp’s and proteins with high homology to known enzymes, structural proteins, matrix proteins, protease inhibitors, mucin-related proteins, immune/defense proteins, calcium-binding protein, and rhamnose-binding protein.

134 Quantitative proteomics classifies 21 footprint-enriched byssal proteins

135 Several proteins were found to be enriched in the footprint relative to the bulk
136 plaque (**Figure 2**). The proteins that were measured to have a footprint-to-bulk plaque
137 fold change ratio (FCR footprint : bulk plaque) > 2 that is statistically significant (p-value
138 < 0.05) are likely to play direct roles in the adhesive mechanism since they are enriched
139 at the interface between the byssus and the substrate.

140 There were 22 significantly enriched footprint proteins identified (**Table 1**). Among
141 these are three variants of Dbfp7 and one variant of Dbfp8. The other proteins are
142 weakly (e-score > e^{-6}), moderately (e^{-30} < e-score < e^{-6}), or strongly (e-score < e^{-30})
143 homologous to known proteins, identified by utilizing the BLASTp algorithm against a
144 clustered non-redundant database (38, 39). Overall, the proteins relatively enriched at
145 the adhesive interface are: Dbfp7, Dbfp8, kielin/chordin-like protein, zonadhesin/IgGFc-
146 binding protein, neurotrypsin-like protein, mucin-like protein, peroxidase, plasminogen-
147 like protein, galaxin-like protein, and several homologues to uncharacterized proteins
148 from other aquatic organisms. Interestingly, some of the proteins contained at least one
149 possible hydroxylated tyrosine residue (i.e. DOPA). None of these proteins, however,
150 were notably abundant with DOPA, corroborating the overall scarcity of DOPA in
151 *Dreissenid* byssus (9) or the limited ability to solubilize DOPA-containing proteins, which
152 can cross-link post-secretion (16, 40–43). Dbfp1 and Dbfp2, previously identified to
153 have the most DOPA (9), were not present in the footprint nor bulk plaque. One
154 transcript (comp50166_c1_seq2-2R) did not have a clear protein-coding open reading
155 frame and was thus excluded as a footprint protein. Parts of the identified peptides of
156 this transcript are probably components of a different protein with a similar transcript
157 sequence.

158 Selection of Dbfp7 as the first footprint protein to characterize

159 Previously, three quagga mussel byssal proteins were identified via a DOPA-
160 specific stain on protein extracted from quagga mussel feet and named Dbfp1, Dbfp2,
161 and Dbfp3 (9). Subsequent characterization of Dbfp1, one of the higher molecular
162 weight DOPA-proteins, has classified it as a cuticle protein or a structural cohesive
163 component (9, 44, 36). The role of Dbfp2 remains unclear (8, 9, 45) and no investigation
164 of Dbfp3 has been done to date.

165 Proteins of similar molecular weight as Dbfp3 were detected in the plaque by
166 MALDI-TOF mass spectrometry and were inferred to contain little to no DOPA (37).
167 Dbfp3 was reclassified as Dbfp7 upon the construction of the quagga mussel foot
168 transcriptome, which revealed significant homology of this protein to the known zebra
169 mussel protein Dpfp7 (8, 46). Herein, the Dbfp7 protein family was identified to be
170 among the proteins that are significantly enriched in the footprint. Taken together this
171 suggests that Dbfp7 plays an important role in byssal adhesion, potentially having a role
172 in bonding to a surface. Dbfp7 was thus selected as the first adhesive protein candidate
173 to be extracted and further characterized.

174 Dbfp7 is polymorphic and DOPA-deficient

175 Dbfp7 was extracted from quagga mussel phenol glands (~ 5 µg per gland) via
176 several steps of selective precipitation and reversed-phase high-pressure liquid
177 chromatography (HPLC) (**Figure S1**) (9). The most abundant residue of Dbfp7 is
178 glycine, followed by significant amounts of proline, asparagine, and tyrosine. There are
179 13 known variants of Dbfp7 detected in naturally secreted byssi, induced byssi, and
180 purified Dbfp7, with lengths ranging from 82 to 132 residues (**Figure 3A**). These
181 variants can be broadly classified as either acidic or basic variants, determined by the
182 theoretical isoelectric point of the sequence. The acidic variants all contain a 28-residue
183 sequence in the C-terminal half of the protein sequence, which is missing from the basic
184 variants. Most of the variation of the Dbfp7 sequence occurs within the first 50 residues;
185 the C-terminal half of Dbfp7 is highly conserved (aside from the presence or absence of
186 the 28-residue sequence).

187 The amount of DOPA in Dbfp7 was found to be notably scarce. Only 1-2 LC-
188 MS/MS sequences of Dbfp7 peptides (in either purified, naturally secreted, or induced
189 instances) confidently contained DOPA, depending on the variant and the extracted
190 pool. The same site of tyrosine hydroxylation was not conserved between induced,
191 purified (pre-secreted), and naturally secreted forms. Most detected hydroxylation
192 modifications were ambiguous (**Figure S4**). Specifically, the identified putative DOPA
193 residues were in spectra of peptides that were not fully fragmented; thus, it is possible
194 the detected hydroxylation was on a different residue within the peptide (e.g.
195 hydroxylysine). Further, purified Dbfp7 is only slightly positively stained with nitroblue

196 tetrazolium (NBT) (**Figure 3B**). The amount of DOPA in Dbfp7 was calculated to be 0.11
197 ± 0.02 mol% (n = 3, s.d.), about 1 DOPA residue per 10 Dbfp7 molecules (**Figure 3C**). It
198 is possible that Dbfp7 and other plaque proteins are hydroxylated extracellularly by
199 tyrosinase, which has been found in the bulk plaque (**Table S1**). Interestingly, the
200 chromatographic fraction of the S2 mixture (**Figure S5C**) eluted before the Dbfp7
201 elution (40-45% acetonitrile), i.e. “pre-Dbfp7 HPLC fraction”, is NBT-positive (**Figure 3B**
202 and **Figure S5A**). This signifies that DOPA can be detected following the extraction
203 method via HPLC. Gel electrophoretic separation of this fraction reveals the presence of
204 low molecular weight proteins with similar weights of purified Dbfp7 (**Figure S5B**). Thus,
205 it is possible that the proteins in the strong low molecular weight NBT-positive band
206 detected by Rzepecki and Waite (9), so-called Dbfp3, was not primarily Dbfp7, but
207 rather was mostly a different protein in the extracted mixture. In any case, the
208 population of Dbfp7 extracted from phenol glands (pre-secretion) characterized herein is
209 deficient in DOPA.
210 Purified forms of Dbfp7 from phenol glands are significantly lower in molecular
211 weight than that of the full theoretical length of the sequence despite the detection of
212 peptides from the full sequence within the purified sample (**Figure S1** and **Figure S2**).
213 Curiously, the localization method of Dbfp7 reveals that although it is overall relatively
214 more abundant in the footprint, the peptides of Dbfp7 detected in the bulk plaque
215 consistently map to the C-terminal portion and the peptides in the footprint mostly map
216 to the N-terminal portion (**Figure S3**). This suggests that Dbfp7 is post-translationally or
217 post-secretionally cleaved. The population of Dbfp7 analyzed herein, which is extracted
218 pre-secretion, also does not contain the full-length molecule (**Figure S2**), therefore,
219 Dbfp7 is likely to be cleaved intracellularly. This raises the possibility that the two
220 portions of Dbfp7 have differing functions, where the N-terminal region interacts with
221 substrates while the C-terminal region is responsible for protein-protein interactions
222 resulting in cohesion between the adhesive and the bulk plaque material. Alternatively, it
223 is possible that C-terminal peptides interacting with the substrate were unable to be
224 extracted from the footprint.
225 Preliminary structural investigations of Dbfp7 reveal both ordered and disordered
226 structure. Due to the presence of multiple variants, structural measurements are an

227 average of the Dbfp7 population extracted from phenol glands. To characterize the
228 structure of Dbfp7, circular dichroism (CD) spectra of Dbfp7 dissolved in 5% acetic acid
229 (**Figure 4A**) were deconvoluted by Contin-LL (47). The proportions of structural features
230 were 3.3 ± 0.3% α-helix, 33 ± 5% β-strand, 20 ± 3% β-turns, and 44 ± 5% disordered
231 (**Figure 4B**). While almost half of the protein was found to be disordered, significant
232 portions of the sample adopted β-strand and β-turn structures. To predict the structure,
233 the AlphaFold protein folding algorithm was used. Due to caveats imposed by the lack
234 of homology of Dbfp7 to other known proteins, pLDDT scores used to determine model
235 confidence were very low (<0.5). The structure is predicted to be entirely disordered;
236 however, the low homology of Dbfp7 to known proteins may result in the prediction
237 algorithm missing ordered regions. Qualitative observations of the model show a C-
238 terminal region that is slightly more compact than the N-terminal portion, which looks
239 relatively extended (**Figure 4C**).

240 <u>Dbfp7 is adhesive in aqueous conditions</u>

241 To assess morphology on a surface and adhesive ability, Dbfp7 was drop casted
242 onto freshly cleaved mica and imaged in aqueous conditions using an atomic force
243 microscope (AFM) in PeakForce tapping mode with quantitative nanomechanical
244 mapping (PFQNM). At 100 µg/mL, a dense layer of round and flat globules (ranging
245 from 3.5 to 35 nm in height) was found throughout the surface (**Figure 4D**).

246 The surface containing Dbfp7 was adhesive, with some portions of relatively
247 lower measured adhesion force that correspond to larger globules in the height map
248 (**Figure 4D** and **Figure 5A**). Overall, Dbfp7 is relatively more adhesive than the control
249 protein, bovine serum albumin (BSA), known to be non-adhesive (**Figure 5C**) (48–51).
250 The average forces of adhesion for Dbfp7 and BSA were measured to be 470 ± 160 pN
251 and 160 ± 140 pN, respectively (s.d. and n = 262,144). Interestingly, the space between
252 Dbfp7 globules (so-called interglobular space) is more adhesive than the globules
253 themselves (**Figure 5B**). This may be due to the inconsistent indentation pressure
254 during scanning, since the setpoint was kept constant during data acquisition.
255 Alternatively, the interglobular space may contain single molecules of Dbfp7 that are
256 more readily available for adhesion to the AFM tip compared to self-assembled
257 globules. This trend is not present in BSA samples (**Figure S6**).

The DMT (Derjaguin-Muller-Toporov) and JKR (Johnson-Kendall-Roberts) models of adhesion predict different contact areas between two surfaces depending on the deformation of the indenting probe (52–54). Depending on the model used, the adhesion energy from the measured adhesion force may vary, and therefore, the appropriate model is required to convert the measured adhesion force to adhesion energy (55–57). The Tabor parameter approximates the appropriate model based on the radius and moduli of the surfaces allowing for the determination of the appropriate theory for the materials in the analyzed system. The Tabor parameter for this experimental set-up was calculated to be ~0.12 (see Supplemental Information for full calculation details). This value means that the contact in this system lies between the characteristic contact regimes described by the two models. Currently, there is no model to adequately describe a system that is characteristic of contact partially described by either the DMT or JKR contact models. Therefore, we report the converted adhesion energy using both the DMT and the JKR models (**Figure 5D**) to compare to adhesive proteins in current literature. The calculated adhesion energy of Dbfp7 is 4.4 ± 1.8 mJ/m^2 (JKR) or 3.3 ± 1.3 mJ/m^2 (DMT) which is ~5 times higher than BSA (0.90 ± 0.89 mJ/m^2 (JKR) or 0.67 ± 0.66 mJ/m^2 (DMT)) (s.d., N = 2,859,269 and 793,084 for Dbfp7 and BSA, respectively). Interestingly, the adhesion energy value for Dbfp7 is in a similar range to the adhesion energy of Mfp3, one of the *Mytilus* adhesive proteins (~3-6 mJ/m^2 determined by surface forces apparatus (SFA) measurements) (14). However, the other known *Mytilus* interfacial protein, Mfp5, remains the strongest known byssal adhesive protein with the most relative amount of DOPA (15 mJ/m^2 and 30 mol% DOPA) (14).

281 *Discussion*

282 Several plaque proteins were identified to be relatively more enriched in the
283 footprint than in the bulk plaque material, suggesting they may play direct roles in
284 plaque-substrate adhesion. Among these, Dbfp7 stood out due to its detection in
285 previous studies on quagga mussel byssal proteins. When extracted from phenol glands
286 (pre-secretion), Dbfp7 adopts a disordered structure with significant proportions of β-
287 strand and β-turn features and contains little to no DOPA. Despite this lack of DOPA,
288 adhesion measurements by AFM performed in aqueous conditions revealed that Dbfp7
289 exhibits wet adhesion similar to Mfp3, one of the marine mussel adhesive proteins.
290 Dbfp7 is thus classified as a DOPA-deficient wet adhesive protein.

291 The marine *Mytilids* and the freshwater *Dreissenids* evolutionarily diverged at the
292 class level; *Dreissenids* have since evolved in brackish water originally and eventually
293 adapted to freshwater habitats (58). It is evident that the significant amount of time
294 between common ancestors gives rise to a variety of differences in the byssal adhesion
295 mechanism. For example, another freshwater byssate *Limnoperna fortunei* (golden
296 mussel) – found in the freshwater systems of Japan, Korea, and Eastern China –
297 diverges from *Mytilus sp*. at the family level and is thus genetically more similar. Indeed,
298 it has been found that the golden mussel byssus contains typical marine mussel
299 adhesive protein domains such as EGF domains, vWFA domains, and GXX motifs (59).
300 Further, DOPA was found in the outer sheath of golden mussel byssal threads and at
301 the bottom of adhesive plaques by NBT staining (59). The presence of DOPA at the
302 adhesive interface suggests DOPA-based interfacial chemistry, however the specific
303 golden mussel footprint proteins have not been characterized yet. In the zebra mussel
304 byssus, DOPA and catechol oxidase was found throughout the plaque, suggesting that
305 some interfacial *Dreissenid* footprint proteins may employ DOPA interfacial chemistry
306 while bulk plaque and thread DOPA-proteins contribute to cross-linking (60). However,
307 the adhesion mechanism of Dbfp7 may be less dependent on DOPA, given the even
308 distribution of DOPA between the thread and plaque.

309 In the marine mussel, the proteins found at the plaque-substrate interface have
310 significantly higher relative amounts of DOPA compared to the bulk plaque and thread
311 proteins. In *Dreissenids*, it was found that peptidyl-DOPA is present in low amounts

312 throughout the byssus, including the thread (9). This suggests that the role of DOPA in
313 the freshwater system is primarily for cross-linking purposes (16, 40–43). Dbfp7 purified
314 from phenol glands of quagga mussels has herein been shown to lack significant
315 amounts of DOPA while being more adhesive than BSA under the same conditions
316 (**Figure 5**). Conversion of the adhesive forces to adhesion energy reveals similar
317 adhesion energy of Dbfp7 compared to one of the marine mussel interfacial proteins,
318 Mfp3. Although similar in molecular weight with abundant glycine, tyrosine, proline, and
319 asparagine residue proportions, Dbfp7 and Mfp3 share very little sequence homology
320 and Mfp3 is more enriched with DOPA (around 10-20 mol%) compared to Dbfp7 (~0.1
321 mol%). The other known interfacial *Mytilus* protein, Mfp5, contains even more DOPA (30
322 mol%) than Mfp3 and is significantly more adhesive than both Mfp3 and Dbfp7 (15
323 mJ/m^2 measured by SFA) (14). It appears that some tyrosine residues in Dbfp7 may be
324 post-secretionally hydroxylated within the distal depression and secreted byssus, since
325 tyrosinases were identified in the bulk plaque (**Table S1**). Still, the DOPA-deficient pre-
326 secretion population of Dbfp7 is adhesive.

327 The mechanism of adhesion for Dbfp7 remains unknown and further studies into
328 specific peptide sequences and post-translational modifications are required to develop
329 a model for the adhesion mechanism. It is possible that in environments with lower ionic
330 strength, as in freshwater habitats, lower amounts of DOPA can achieve similar
331 adhesive strength. Further, several efforts are being made to understand the role of
332 lysine and other cationic moieties in conjunction with DOPA-based adhesion,
333 particularly in cation-pi interactions for cross-linking and complex coacervation (34, 61–
334 67). It is unclear whether the dihydroxyl moiety in catechol is necessary for this
335 interaction or if the phenyl moiety in residues such as tyrosine, phenylalanine, and
336 tryptophan is sufficient (68, 69). Charged residues may also play a role in dislodging
337 surface-bound water molecules and surface ions to allow for direct contact with a
338 surface (34). Indeed, Dbfp7 contains significant amounts of aromatic residues tyrosine
339 and tryptophan, as well as positively charged lysine (**Figure 3A**).

340 Dbfp7 is polymorphic with up to 13 detected variants. Several genes of the zebra
341 mussel homologue of Dbfp7, Dpfp7, have been identified in multiple regions of the
342 zebra mussel genome (70). Mfp3 is similarly polymorphic, with up to 35 known variants

343 encoded throughout the *Mytilus sp.* genome (5). The existence of multiple variants of a
344 gene that is preserved several times in the genome suggests vital importance.
345 Particularly, polymorphism of an interfacial protein may enhance the versatility of
346 adhesion to different kinds of surfaces (3, 5, 8, 16). Further, Mfp3 is known to exist as
347 two populations, Mfp3S and Mfp3F, so-called the slow and fast variants due to their
348 elution time in reversed-phase HPLC, thereby differing in hydrophobicity. Mfp3S was
349 found to be more resistant to oxidation and retains adhesion when pH is equilibrated to
350 seawater levels (7, 71). The role of the two variant types of Dbfp7 (acidic and basic) is
351 currently unclear and may: (i) function similarly to the Mfp3 variants, (ii) have different
352 roles in the footprint-bulk plaque and footprint-substrate interfaces, or (iii) contribute to
353 spreading behaviour on a surface by the formation of complex coacervates during
354 secretion (72–74). Encoding and synthesizing these two peptide components in the
355 same transcript may have the advantage of maintaining stoichiometric proportions.
356 The quagga mussel footprint contains 20 proteins in addition to Dbfp7 that
357 contribute to byssal adhesion, possibly in interfacial interactions (**Table 1**). Further
358 investigation is needed to understand the interactions between these proteins with each
359 other, with bulk plaque proteins, and with adherend substrates. Of particular interest are
360 the zonadhesin/IgGFc-binding proteins, homologues of which were found in the sea star
361 (*Asteria rubens*) adhesive footprint (75). Further, kielin/chordin-like proteins match the
362 molecular weights of interfacial plaque proteins identified by MALDI-TOF (37). With the
363 advent of high-throughput sequencing techniques, the library of proteins found in
364 bioadhesive systems is vast. Little has been done to localize these proteins at the direct
365 adhesive-substrate interface *in situ*, with a larger current focus on bulk cohesive
366 properties than on interfacial adhesion chemistry. Localization of proteins at direct
367 adhesive-substrate interfaces will provide a smaller subset to analyze for understanding
368 the fundamental mechanisms of bioadhesion in aqueous environments.
369 It is difficult to directly compare adhesive measurements of Dbfp7 to other studies
370 since the methods of wet adhesive protein characterization are varied. SFA developed
371 by Israelachvili and applied by Waite and others to marine byssal proteins has been the
372 predominant method of adhesive measurements (14, 34, 69, 76–79). This unique
373 instrument is not as widely implemented compared to AFM. Although similar in

374 fundamental operation (i.e. generation and analysis of submicron contact force-distance
375 curves), the planar scale of these two systems is different, with SFA analyzing at the
376 squared milli- to centimetre contact area range and AFM analyzing at the squared nano-
377 to micrometre contact area range. The classical models of contact (Hertz, DMT, JKR,
378 etc.) may allow for the comparison of adhesion energies obtained from different
379 systems; however, the physics at these two scales may be fundamentally different and
380 thus may not be directly comparable. To date, the adhesion in systems that lie between
381 DMT and JKR contact models is yet to be fully understood (55, 56, 80, 81). Further
382 complications arise when the two contacting surfaces are not entirely flat or smooth (57,
383 82). Advancements in theoretical contact physics at the nanoscale are needed to
384 harmonize any discrepancies that may arise from measuring adhesion at differing size
385 scales. The problem of scale may be circumvented with the use of colloidal probe
386 technique, allowing for the analysis of adhesion at the micrometre contact area scale in
387 AFM (83, 84). This technique, however, cannot be used for concurrent imaging and
388 characterization of mechanical properties. Further, the adhesion measurements
389 obtained herein presumably represent adhesion of Dbfp7 with the silicon nitride AFM tip.
390 It is possible that some adhesion measurements were from Dbfp7 bound to the tip,
391 resulting in a measurement of the interactions between Dbfp7-to-Dbfp7 or Dbfp7-to-
392 mica. Since the protein seems to aggregate resulting in a non-uniform molecular layer
393 and due to the limited lateral resolution of AFM imaging, these possible interactions may
394 contribute to the observed adhesion average.

395 This study highlights the importance of studying aqueous bioadhesive proteins
396 from a diversity of organisms. To our knowledge, Dbfp7 is the first freshwater wet
397 adhesive protein to be functionally characterized. The lack of DOPA in this protein is
398 interesting but not shocking when considering the evolutionary history of *Dreissenids*
399 compared to the other bioadhesive systems studied so far. The inclusion of Dbfp7 (and
400 potentially others from the 20 footprint proteins herein localized) to the repertoire of wet
401 bioadhesive proteins will allow for the identification of the fundamental properties
402 required to achieve biocompatible wet adhesion for the development of bio-inspired wet
403 adhesive materials. Further, understanding the specific mechanism of adhesion
404 employed by *Dreissenids* that are invasive species to the Great Lakes basin and

405 connected waterways in North America will aid in the development of anti-fouling
406 strategies (85).
407

408 *Materials and Methods*

409 Quagga mussel collection and maintenance

410 Freshwater mussels were harvested from Lake Ontario at Port Credit Harbour
411 Marina in Mississauga, Ontario. Live mussels were cleaned and sorted by species
412 (quagga mussels and zebra mussels) and transferred to tanks with circulating artificial
413 lake water (0.30 mM sodium bicarbonate, 0.13 mM potassium bicarbonate, 0.35 mM
414 sodium chloride, 0.67 mM magnesium sulfate, 0.08 mM magnesium chloride, 1.47 mM
415 calcium carbonate) at 12ºC and fed powdered green algae.

416 Plaque protein collection

417 Quagga mussels were first detached from their original substrates (tank walls or
418 other mussels), secured into individual cages with glass slides, and allowed to lay byssi
419 overnight. Mussels were gently detached from the substrates by cutting the byssal
420 threads, leaving the plaque intact on the glass slide. Bulk plaque material was scraped
421 off with a razor blade and collected in a pool of extraction buffer (composed of 200 mM
422 sodium borate, 4 M urea, 1 mM potassium cyanide, 1 mM ethylenediaminetetraacetic
423 acid, and 10 mM ascorbic acid, at pH 8.0). Extraction buffer was deposited onto the
424 footprint residue remaining on the slide, incubated for 1-2 minutes, then collected.
425 Samples were homogenized in a 1 mL tissue grinder on ice, centrifuged at 17,000 x g
426 for eight minutes at 4ºC, then flash frozen for storage until analysis. Amounts of bulk
427 plaque and footprint pools were normalized by weight (resulting in 25 bulk plaques and
428 400 footprints in total for comparative analysis).

429 Tandem mass spectrometry on digested peptides extracted from freshly secreted
430 byssus

431 The bulk plaque and the footprint pools were digested with 13 ng/µL trypsin
432 (Porcine, sequencing grade, Promega) overnight at 37ºC. Following digestion, the bulk
433 plaque peptides were functionalized with TMT-2plex TMT-131 and footprint peptides
434 were functionalized with TMT-2plex TMT-126. The peptide pools were then pooled and
435 loaded onto a 100 µm internal diameter (ID) pre-column (Dionex) at 4 µL/min and
436 separated over a 50 µm ID analytical column (C18 2 µm, Dionex). The peptides were
437 eluted on a 0 to 35% acetonitrile gradient with an EASY-nLC 1000 nano-

438 chromatography pump (Thermo Fisher, Odense Denmark). Data was acquired at
439 70,000 FWHM resolution in the MS mode and 17,500 FWHM resolution in the MS/MS
440 mode. A total of 10 MS/MS scans were obtained per MS cycle.

441 *In silico* methods for protein identification, selection, and sequence analysis

442 LC-MS/MS data was analyzed with PEAKS Studio 10.5 (Bioinformatics Solutions
443 Inc.) and Scaffold 5.0 (Proteome Software Inc.). *De novo* sequences derived from
444 MS/MS data were matched against the quagga mussel foot transcriptome (8) with
445 tyrosine hydroxylation to DOPA, deamidation, oxidation, and carbamidomethylation set
446 as variable modifications. Parent ion and fragment ion mass tolerances were set to 5
447 PPM and 0.01 Da, respectively. Acceptance criteria for identified proteins were peptide
448 logP ≥ 15, protein –10 logP ≥ 50, and *de novo* average local confidence (ALC) score ≥
449 80%, with at least two peptide spectra per identification.

450 Scaffold Q+ in Scaffold 5.0 was used to quantitate label-based quantitation
451 peptide and protein identifications. Peptide identifications were accepted if they could be
452 established at ≥ 75.0% probability to achieve an FDR < 0.1% and contained at least two
453 identified peptides. Normalization against the reference (bulk plaque) were performed
454 iteratively across samples and spectra on intensities, as described in (86). Spectra data
455 were log-transformed and weighted by an adaptive intensity weighting algorithm.
456 Differentially expressed proteins were determined by applying the permutation test with
457 unadjusted significance level $p < 0.05$ corrected by the Benjamini-Hochberg procedure.

458 The Protein Basic Local Alignment Search Tool (BLASTp) algorithm was applied
459 on the identified proteins of interest against a clustered non-redundant database (38,
460 39) for homology assessment. Alignment of sequences were visualized in Jalview
461 2.11.3.3 using the Clustal Omega multiple sequence alignment program. The
462 ProtParam online tool (Expasy) was used to calculate residue frequency, molecular
463 weight, and isoelectric point of full-length protein sequences obtained from virtual
464 translation of the open-reading frame of identified transcripts.

465 The method for analyzing tyrosine hydroxylation was categorized based on the
466 level of confidence in the identified modification. A modification was considered
467 confident if the tyrosine residue (Y) was highlighted with a specific residue number by
468 the PEAKS PTM algorithm. It was classified as semi-confident if no number was

469 indicated, but the spectrum contained a Y+16.99 m/z modification in both the b- and y-
470 ions, indicating hydroxylation at that residue. Finally, a non-confident classification was
471 assigned if a number was not indicated and the spectrum only showed the Y+16.99 m/z
472 within an unfragmented peptide, suggesting that the tyrosine residue was not
473 individually sequenced.

474 Purification of Dbfp7

475 Dbfp7 was purified from quagga mussel phenol glands (**Figure S1**). The crude
476 protein extraction method was adapted from (9). Phenol glands were dissected out of
477 freshly harvested quagga mussels and homogenized in 5% acetic acid with 10 μM
478 pepstatin and leupeptin protease inhibitors. The mixture was centrifuged at 20,000 x g
479 for 40 minutes at 4ºC. The pellet (P1) was then homogenized in 5% acetic acid and 8 M
480 urea. The mixture is then centrifuged at 20,000 x g for 40 minutes at 4ºC. The
481 supernatant (S2), i.e. the urea-soluble proteins, was then mixed with mobile phase
482 (0.1% trifluoroacetic acid (TFA)) and injected into a C4 reversed-phase column (XBridge
483 Protein BEH C4, 300 Å). The eluent at 40 to 45% acetonitrile (with 0.1% TFA) was
484 collected, lyophilized, and stored at -80ºC until analysis.

485 Structure Prediction with AlphaFold

486 The structure of Dbfp7 variant 1 was predicted with AlphaFold2 protein structure
487 prediction (87). The query sequence was input in the ColabFold v1.5.5 python notebook
488 and the resulting structures were visualized with ChimeraX v1.8.

489 Gel electrophoresis

490 Samples were separated by molecular weight via gel electrophoresis in Bolt 12%
491 Bis-Tris precast gels, using Bolt MES-SDS running buffer and Bolt LDS sample buffer.
492 Gels were run at constant 165 V voltage for 40 minutes. The gels were fixed in 40%
493 methanol + 10% acetic acid and stained with Coomassie Brilliant Blue R-250 for 1 hour.
494 Gels were destained and visualized with a digital camera.

495 ESI mass spectrometry

496 Dbfp7 was dissolved in 5% acetic acid at 400 μg/mL and ionized by electrospray
497 ionization. The sample was analyzed with an Agilent 6538 UHD hybrid quadrupole time-

498 of-flight mass spectrometer. The mass spectrum was processed using the Maximum
499 Entropy algorithm implemented in the MassHunter BioConfirm software package.

500 Nitroblue tetrazolium staining for DOPA detection

501 NBT was used to detect and quantify DOPA amounts. This protocol was adapted
502 from (9, 88). Samples were prepared by adding 20 µL to 0.17 mM NBT in 2 M K-
503 glycinate, then incubating at room temperature in the dark for 1 hour. The absorbance at
504 530 nm was measured and compared to a calibration curve generated using samples
505 prepared with standard amounts of peptidyl DOPA. Peptidyl DOPA standards were
506 synthesized by Biomatik and include the first 13 residues of Dbfp7, with the penultimate
507 tyrosine replaced with DOPA.

508 Dot blots were prepared by depositing 10 µL of sample onto a nitrocellulose
509 membrane and allowing it to dry in air for 30 minutes. The membrane was then rinsed
510 with potassium glycinate for 30 minutes, then stained with 0.24 mM NBT for 1.5 hours in
511 the dark, then rinsed with 0.2 M sodium borate for 1 hour.

512 Sample preparation and spectra analysis for circular dichroism

513 To characterize the secondary structure of purified Dbfp7, far-UV circular
514 dichroism was performed. The CD spectra was recorded using a Jasco
515 spectropolarimeter, with a 2-nm bandwidth, scanning speed of 20 nm/min at a spectral
516 resolution of 1.0 nm. The scans were averaged over ten scans, and the data was
517 smoothed. The CD spectra of the buffer was recorded and manually subtracted from
518 sample spectra. The secondary structure was characterized by computational analysis
519 of the spectra using the Contin-LL program from the Dichroweb package (47).
520 Measured ellipticity was normalized to the molecular weight, pathlength, and
521 concentration of the sample to get the mean residue ellipticity (deg*cm^2/dmol). The
522 average molecular weight of 7.2 kDa, as determined by mass spectrometry, was used.

523 Sample preparation for atomic force microscopy

524 10 µL of sample was deposited onto freshly cleaved mica (V1 high grade) and
525 incubated in a humidified chamber for 20 minutes. Residual protein was thoroughly
526 washed away with blank solution (e.g. 5% acetic acid for Dbfp7 samples dissolved in

527 5% acetic acid). A droplet of deionized water was dropped onto the sample and placed
528 in a fluid cell for AFM imaging in aqueous conditions.

529 Imaging and adhesion force mapping via AFM PFQNM

530 Samples were imaged with a MultiMode Atomic Force Microscope equipped with
531 a Nanoscope 6 controller operated via Nanoscope 10.0 software in PeakForce tapping
532 mode with quantitative nanomechanical mapping (PFQNM). SCANASYST-FLUID
533 probes with 20 nm (nominal) silicon nitride tips were calibrated on blank mica in water,
534 resulting in calibrated spring constants around 0.7 N/m. The images were taken at 512-
535 line resolution at 1.0 Hz line rate. ScanAsyst mode allows for automatic control of
536 setpoint, gain, and scan rate. Initial images were taken with ScanAsyst auto-control on
537 to determine the ideal setpoint for the sample. ScanAsyst auto-control was
538 subsequently turned off to allow for direct pixel-to-pixel comparison of nanomechanical
539 properties derived from the collected force-distance curves. PeakForce data was
540 captured at a rate such that each height pixel has a corresponding force-distance curve
541 saved. Images were analyzed using the Nanoscope Analysis 3.0 software. The
542 individual curves for the entire map were baseline-corrected and moduli were fitted
543 using the JKR contact model. Adhesion was calculated using the positive-slope
544 algorithm.
545

Author Contributions

A.R.O., R.H., D.J.R., J.N., and E.D.S. designed research; A.R.O., R.H., D.J.R., and J.N. performed research; A.R.O., R.H., D.J.R., J.N., K.M.M.C., and E.D.S. analyzed data; and A.R.O., R.H., K.M.M.C., and E.D.S. wrote the paper.

Acknowledgements

This research was supported by Discovery Grant #342455 to E.D.S. from the Natural Sciences and Engineering Research Council of Canada (NSERC) (RGPIN-2019-06210), Post-Graduate Scholarship – Doctoral (PGS-D) to A.R.O. from NSERC, and the Queen Elizabeth II Graduate Scholarship in Science and Technology (QEII-GSST) to A.R.O. from the Government of Ontario. The authors thank the SickKids Proteomics, Analytics, Robotics & Chemical Biology Centre for assistance with LC-MS/MS data collection and interpretation, the Advanced Instrumentation for Molecular Structure Laboratory for ESI MS, and the SickKids Structural and Biophysical Core Facility for CD and HPLC. Special thanks are extended to Ryan Lee Chan for his assistance with AFM. The authors also gratefully acknowledge Dr. Magdalena Wojtas for her valuable insights and advice throughout the project.

Competing Interest Statement

The authors declare no competing interest.

Abbreviations/Acronyms/Initialisms

DOPA = 3,4-dihydroxyphenylalanine
Dbfp = *Dreissena bugensis* foot protein
Dpfp = *Dreissena polymorpha* foot protein
MALDI-TOF = matrix-assisted laser desorption/ionization time-of-flight
LC-MS/MS = liquid chromatography tandem mass spectrometry
FP = footprint
BP = bulk plaque
IND = induced byssus
TMT = tandem mass tag
BLAST = basic local alignment search tool
KCl = potassium chloride
FCR = fold change ratio
HPLC = high-pressure liquid chromatography
NBT = nitroblue tetrazolium
pLDDT = predicted local distance difference test
AFM = atomic force microscope
CD = circular dichroism
BSA = bovine serum albumin
DMT = Derjaguin-Muller-Toporov
JKR = Johnson-Kendall-Roberts
SFA = surface forces apparatus
ID = internal diameter
TFA = trifluoroacetic acid

References

1. C. Liu, Comparative Proteomics for an In-Depth Understanding of Bioadhesion Mechanisms and Evolution across Metazoans. *Journal of Proteomics*, **256**, 104506 (2022). https://doi.org/10.1016/j.jprot.2022.104506.
2. N. Farsad, E. D. Sone, Zebra Mussel Adhesion: Structure of the Byssal Adhesive Apparatus in the Freshwater Mussel, *Dreissena Polymorpha*. *Journal of Structural Biology*, **177**(3), 613–620 (2012). https://doi.org/10.1016/j.jsb.2012.01.011.
3. H. Zhao, J. H. Waite, Linking Adhesive and Structural Proteins in the Attachment Plaque of *Mytilus Californianus*. *Journal of Biological Chemistry*, **281**(36), 26150–26158 (2006). https://doi.org/10.1074/jbc.M604357200.
4. J. H. Waite, Adhesion a La Moule. *Integrative and Comparative Biology*, **42**(6), 1172–1180 (2002). https://doi.org/10.1093/icb/42.6.1172.
5. R. Y. Floriolli, J. Von Langen, J. H. Waite, Marine Surfaces and the Expression of Specific Byssal Adhesive Protein Variants in *Mytilus*. *Mar. Biotechnol.*, **2**(4), 352–363 (2000). https://doi.org/10.1007/s101269900032.
6. M. A. McCartney, Structure, Function and Parallel Evolution of the Bivalve Byssus, with Insights from Proteomes and the Zebra Mussel Genome. *Phil. Trans. R. Soc. B*, **376**(1825), 20200155 (2021). https://doi.org/10.1098/rstb.2020.0155.
7. D. G. DeMartini, J. M. Errico, S. Sjoestroem, A. Fenster, J. H. Waite, A Cohort of New Adhesive Proteins Identified from Transcriptomic Analysis of Mussel Foot Glands. *J. R. Soc. Interface*, **14**(131), 20170151 (2017). https://doi.org/10.1098/rsif.2017.0151.
8. D. J. Rees, A. Hanifi, A. Obille, R. Alexander, E. D. Sone, Fingerprinting of Proteins That Mediate Quagga Mussel Adhesion Using a De Novo Assembled Foot Transcriptome. *Sci Rep*, **9**(1), 6305 (2019). https://doi.org/10.1038/s41598-019-41976-7.
9. L. M. Rzepecki, J. H. Waite, The Byssus of the Zebra Mussel, *Dreissena Polymorpha*. II: Structure and Polymorphism of Byssal Polyphenolic Protein Families. *Mol Mar Biol Biotechnol.* 2(5), 267–279 (1993).
10. J. H. Waite, M. L. Tanzer, Polyphenolic Substance of *Mytilus Edulis*: Novel Adhesive Containing L-Dopa and Hydroxyproline. *Science*, **212**(4498), 1038–1040 (1981). https://doi.org/10.1126/science.212.4498.1038.
11. M. Yu, J. Hwang, T. J. Deming, Role of l -3,4-Dihydroxyphenylalanine in Mussel Adhesive Proteins. *J. Am. Chem. Soc.*, **121**(24), 5825–5826 (1999). https://doi.org/10.1021/ja990469y.
12. H. Lee, N. F. Scherer, P. B. Messersmith, Single-Molecule Mechanics of Mussel Adhesion. *Proc. Natl. Acad. Sci. U.S.A.*, **103**(35), 12999–13003 (2006). https://doi.org/10.1073/pnas.0605552103.
13. B. K. Ahn, Perspectives on Mussel-Inspired Wet Adhesion. *J. Am. Chem. Soc.*, **139**(30), 10166–10171 (2017). https://doi.org/10.1021/jacs.6b13149.
14. J. H. Waite, Mussel Adhesion – Essential Footwork. *Journal of Experimental Biology*, **220**(4), 517–530 (2017). https://doi.org/10.1242/jeb.134056.
15. T. H. Anderson *et al*., The Contribution of DOPA to Substrate–Peptide Adhesion and Internal Cohesion of Mussel-Inspired Synthetic Peptide Films. *Adv Funct Materials*, **20**(23), 4196–4205 (2010). https://doi.org/10.1002/adfm.201000932.

632 16. R. J. Stewart, T. C. Ransom, V. Hlady, Natural Underwater Adhesives. *J Polym Sci B*
633 *Polym Phys*, **49**(11), 757–771 (2011). https://doi.org/10.1002/polb.22256.
634 17. M. L. B. Palacio, B. Bhushan, Bioadhesion: A Review of Concepts and Applications.
635 *Phil. Trans. R. Soc. A.*, **370**(1967), 2321–2347 (2012).
636 https://doi.org/10.1098/rsta.2011.0483.
637 18. Y. Kan, Z. Wei, Q. Tan, Y. Chen, Inter- and Intramolecular Adhesion Mechanisms of
638 Mussel Foot Proteins. *Sci. China Technol. Sci.*, **63**(9), 1675–1698 (2020).
639 https://doi.org/10.1007/s11431-019-1541-8.
640 19. B. P. Lee, P. B. Messersmith, J. N. Israelachvili, J. H. Waite, Mussel-Inspired
641 Adhesives and Coatings. *Annu. Rev. Mater. Res.*, **41**(1), 99–132 (2011).
642 https://doi.org/10.1146/annurev-matsci-062910-100429.
643 20. M. Mehdizadeh, J. Yang, Design Strategies and Applications of Tissue Bioadhesives.
644 *Macromolecular Bioscience*, **13**(3), 271–288 (2013).
645 https://doi.org/10.1002/mabi.201200332.
646 21. S. Moulay, Dopa/Catechol-Tethered Polymers: Bioadhesives and Biomimetic
647 Adhesive Materials. *Polymer Reviews*, **54**(3), 436–513 (2014).
648 https://doi.org/10.1080/15583724.2014.881373.
649 22. P. Kord Forooshani, B. P. Lee, Recent Approaches in Designing Bioadhesive
650 Materials Inspired by Mussel Adhesive Protein. *J. Polym. Sci. Part A: Polym. Chem.*,
651 **55**(1), 9–33 (2017). https://doi.org/10.1002/pola.28368.
652 23. L. Li, H. Zeng, Marine Mussel Adhesion and Bio-Inspired Wet Adhesives.
653 *Biotribology*, **5**, 44–51 (2016). https://doi.org/10.1016/j.biotri.2015.09.004.
654 24. A. J. Vernengo, “Adhesive Materials for Biomedical Applications” in *Adhesives -*
655 *Applications and Properties*, A. Rudawska, Ed., (InTech, 2016).
656 https://doi.org/10.5772/64958.
657 25. G. P. Maier, C. M. Bernt, A. Butler, Catechol Oxidation: Considerations in the Design
658 of Wet Adhesive Materials. *Biomater. Sci.*, **6**(2), 332–339 (2018).
659 https://doi.org/10.1039/C7BM00884H.
660 26. S. Basak, Co-Evolving with Nature: The Recent Trends on the Mussel-Inspired
661 Polymers in Medical Adhesion. *Biotechnol Bioproc E*, **26**(1), 10–24 (2021).
662 https://doi.org/10.1007/s12257-020-0234-z.
663 27. G. M. Taboada *et al*., Overcoming the Translational Barriers of Tissue Adhesives.
664 *Nat Rev Mater*, **5**(4), 310–329 (2020). https://doi.org/10.1038/s41578-019-0171-7.
665 28. J. H. Waite, M. J. Harrington, Following the Thread: *Mytilus* Mussel Byssus as an
666 Inspired Multi-Functional Biomaterial. *Can. J. Chem.*, **100**(3), 197–211 (2022).
667 https://doi.org/10.1139/cjc-2021-0191.
668 29. X. Ma *et al*., Hydrogels for Underwater Adhesion: Adhesion Mechanism, Design
669 Strategies and Applications. *J. Mater. Chem. A*, **10**(22), 11823–11853 (2022).
670 https://doi.org/10.1039/D2TA01960D.
671 30. J. Yu, W. Wei, E. Danner, J. N. Israelachvili, J. H. Waite, Effects of Interfacial Redox
672 in Mussel Adhesive Protein Films on Mica. *Advanced Materials*, **23**(20), 2362–2366
673 (2011). https://doi.org/10.1002/adma.201003580.
674 31. J. Yu *et al*., Mussel Protein Adhesion Depends on Interprotein Thiol-Mediated Redox
675 Modulation. *Nat Chem Biol*, **7**(9), 588–590 (2011).
676 https://doi.org/10.1038/nchembio.630.

32. R. Mirshafian, W. Wei, J. N. Israelachvili, J. H. Waite, α,β-Dehydro-Dopa: A Hidden Participant in Mussel Adhesion. *Biochemistry*, **55**(5), 743–750 (2016). https://doi.org/10.1021/acs.biochem.5b01177.
33. R. Chollakup, J. B. Beck, K. Dirnberger, M. Tirrell, C. D. Eisenbach, Polyelectrolyte Molecular Weight and Salt Effects on the Phase Behavior and Coacervation of Aqueous Solutions of Poly(Acrylic Acid) Sodium Salt and Poly(Allylamine) Hydrochloride. *Macromolecules*, **46**(6), 2376–2390 (2013). https://doi.org/10.1021/ma202172q.
34. G. P. Maier, M. V. Rapp, J. H. Waite, J. N. Israelachvili, A. Butler, Adaptive Synergy between Catechol and Lysine Promotes Wet Adhesion by Surface Salt Displacement. *Science* **349**, 628–632 (2015).
35. X. Ou *et al*., Structure and Sequence Features of Mussel Adhesive Protein Lead to Its Salt-Tolerant Adhesion Ability. *Sci. Adv.*, **6**(39), eabb7620 (2020). https://doi.org/10.1126/sciadv.abb7620.
36. K. E. Anderson, J. H. Waite, Immunolocalization of Dpfp1, a Byssal Protein of the Zebra Mussel *Dreissena Polymorpha*. *Journal of Experimental Biology*, **203**(20), 3065–3076 (2000). https://doi.org/10.1242/jeb.203.20.3065.
37. D. J. Rees, A. Hanifi, J. Manion, A. Gantayet, E. D. Sone, Spatial Distribution of Proteins in the Quagga Mussel Adhesive Apparatus. *Biofouling*, **32**(2), 205–213 (2016). https://doi.org/10.1080/08927014.2015.1135426.
38. M. Steinegger, J. Söding, MMseqs2 Enables Sensitive Protein Sequence Searching for the Analysis of Massive Data Sets. *Nat Biotechnol*, **35**(11), 1026–1028 (2017). https://doi.org/10.1038/nbt.3988.
39. S. F. Altschul, W. Gish, W. Miller, E. W. Myers, D. J. Lipman, Basic Local Alignment Search Tool.
40. B. Liu, L. Burdine, T. Kodadek, Chemistry of Periodate-Mediated Cross-Linking of 3,4-Dihydroxylphenylalanine-Containing Molecules to Proteins. *J. Am. Chem. Soc.*, **128**(47), 15228–15235 (2006). https://doi.org/10.1021/ja065794h.
41. L. A. Burzio, J. H. Waite, Reactivity of Peptidyl-tyrosine to Hydroxylation and Cross-linking. *Protein Science*, **10**(4), 735–740 (2001). https://doi.org/10.1110/ps.44201.
42. N. Holten-Andersen *et al*., pH-Induced Metal-Ligand Cross-Links Inspired by Mussel Yield Self-Healing Polymer Networks with near-Covalent Elastic Moduli. *Proc. Natl. Acad. Sci. U.S.A.*, **108**(7), 2651–2655 (2011). https://doi.org/10.1073/pnas.1015862108.
43. M. Mesko *et al*., Catechol-Vanadium Binding Enhances Cross-Linking and Mechanics of a Mussel Byssus Coating Protein. *Chem. Mater.*, **33**(16), 6530–6540 (2021). https://doi.org/10.1021/acs.chemmater.1c02063.
44. K. E. Anderson, J. H. Waite, Biochemical Characterization of a Byssal Protein from *Dreissena Bugensis* (Andrusov). *Biofouling*, **18**(1), 37–45 (2002). https://doi.org/10.1080/08927010290017716.
45. A. Gantayet, L. Ohana, E. D. Sone, Byssal Proteins of the Freshwater Zebra Mussel, *Dreissena Polymorpha*. *Biofouling*, **29**(1), 77–85 (2013). https://doi.org/10.1080/08927014.2012.746672.

46. A. Gantayet, D. J. Rees, E. D. Sone, Novel Proteins Identified in the Insoluble Byssal Matrix of the Freshwater Zebra Mussel. *Mar Biotechnol*, **16**(2), 144–155 (2014). https://doi.org/10.1007/s10126-013-9537-9.
47. A. J. Miles, S. G. Ramalli, B. A. Wallace, DichroWeb, a Website for Calculating Protein Secondary Structure from Circular Dichroism Spectroscopic Data. *Protein Science*, **31**(1), 37–46 (2022). https://doi.org/10.1002/pro.4153.
48. J. J. Valle-Delgado *et al*., Interactions between Bovine Serum Albumin Layers Adsorbed on Different Substrates Measured with an Atomic Force Microscope. *Phys. Chem. Chem. Phys.*, **6**(7), 1482–1486 (2004). https://doi.org/10.1039/B314060C.
49. M. S. Wang, L. B. Palmer, J. D. Schwartz, A. Razatos, Evaluating Protein Attraction and Adhesion to Biomaterials with the Atomic Force Microscope. *Langmuir*, **20**(18), 7753–7759 (2004). https://doi.org/10.1021/la049849+.
50. Y. Yu, P.Q. Ying, G. Jin, Competitive Adsorption between Bovine Serum Albumin and Collagen Observed by Atomic Force Microscope. *Chinese Chemical Letters*, **15**(12), 1465–1468 (2004).
51. A. P. Serro, K. Degiampietro, R. Colaço, B. Saramago, Adsorption of Albumin and Sodium Hyaluronate on UHMWPE: A QCM-D and AFM Study. *Colloids and Surfaces B: Biointerfaces*, **78**(1), 1–7 (2010). https://doi.org/10.1016/j.colsurfb.2010.01.022.
52. B.V. Derjaguin, V.M. Muller, Y.P. Toporov, Effect of Contact Deformations on the Adhesion of Particles. *Journal of Colloid and Interface Science*, **53**(2), 314–326 (1974).
53. V. M. Muller, B.V. Derjaguin, Y. P. Toporov, On Two Methods of Calculation of the Force of Sticking of an Elastic Sphere to a Rigid Plane. *Colloids and Surfaces*, **7**, 251–259 (1983).
54. K. L. Johnson, K. Kendall, A. D. Roberts, Surface Energy and the Contact of Elastic Solids. *Proc. R. Soc. Lond. A*, **324**, 301–313 (1971).
55. D. S. Grierson, E. E. Flater, R. W. Carpick, Accounting for the JKR–DMT Transition in Adhesion and Friction Measurements with Atomic Force Microscopy. *Journal of Adhesion Science and Technology*, **19**(3–5), 291–311 (2005). https://doi.org/10.1163/1568561054352685.
56. X. Gao, F. Hao, Z. Huang, D. Fang, Mechanics of Adhesive Contact at the Nanoscale: The Effect of Surface Stress. *International Journal of Solids and Structures*, **51**(3–4), 566–574 (2014). https://doi.org/10.1016/j.ijsolstr.2013.10.017.
57. S.-H. Kim *et al*., An Experimental and Numerical Study on Adhesion Force at the Nanoscale. *Nanoscale Adv.*, **6**(8), 2013–2025 (2024). https://doi.org/10.1039/D3NA01044A.
58. A. Y. Karatayev, D. Boltovskoy, L. E. Burlakova, D. K. Padilla, Parallels and Contrasts Between *Limnoperna Fortunei* and Species of *Dreissena*. In *Limnoperna Fortunei*, D. Boltovskoy, Ed. (Springer, Cham, 2015), pp. 261–297. https://doi.org/10.1007/978-3-319-13494-9_15.
59. S. Li, Z. Xia, Y. Chen, Y. Gao, A. Zhan, Byssus Structure and Protein Composition in the Highly Invasive Fouling Mussel *Limnoperna Fortunei*. *Front. Physiol.*, **9**, 418 (2018). https://doi.org/10.3389/fphys.2018.00418.
60. N. Farsad, T. W. Gilbert, E. D. Sone, Adhesive Structure of the Freshwater Zebra Mussel, *Dreissena polymorpha*. *Mater. Res. Soc. Symp. Proc.*, *1187-KK02-03* (2009).

61. S. Kim *et al*., Cation–π Interaction in DOPA-Deficient Mussel Adhesive Protein Mfp-1. *J. Mater. Chem. B*, **3**(5), 738–743 (2015). https://doi.org/10.1039/C4TB01646G.
62. M. A. Gebbie *et al*., Tuning Underwater Adhesion with Cation–π Interactions. *Nature Chem*, **9**(5), 473–479 (2017). https://doi.org/10.1038/nchem.2720.
63. L. Fischer *et al*., Sequence-Defined Positioning of Amine and Amide Residues to Control Catechol Driven Wet Adhesion. *Chem. Sci.*, **11**(36), 9919–9924 (2020). https://doi.org/10.1039/D0SC03457F.
64. Y. Li *et al*., Molecular Design Principles of Lysine-DOPA Wet Adhesion. *Nat Commun*, **11**(1), 3895 (2020). https://doi.org/10.1038/s41467-020-17597-4.
65. Y. Mu, P. Mu, X. Wu, X. Wan, The Two Facets of the Synergic Effect of Amine Cation and Catechol on the Adhesion of Catechol in Underwater Conditions. *Applied Surface Science*, **530**, 146973 (2020). https://doi.org/10.1016/j.apsusc.2020.146973.
66. M. Shin, J. Y. Shin, K. Kim, B. Yang, J. W. Han, N.-K. Kim, H. J. Cha, The Position of Lysine Controls the Catechol-Mediated Surface Adhesion and Cohesion in Underwater Mussel Adhesion. *Journal of Colloid and Interface Science*, **563**, 168–176 (2020). https://doi.org/10.1016/j.jcis.2019.12.082.
67. B. D. B. Tiu, P. Delparastan, M. R. Ney, M. Gerst, P. B. Messersmith, Cooperativity of Catechols and Amines in High-Performance Dry/Wet Adhesives. *Angew Chem Int Ed*, **59**(38), 16616–16624 (2020). https://doi.org/10.1002/anie.202005946.
68. X. Zhu, C. Wei, H. Chen, C. Zhang, H. Peng, D. Wang, J. Yuan, J. H. Waite, Q. Zhao, A Cation-Methylene-Phenyl Sequence Encodes Programmable Poly(Ionic Liquid) Coacervation and Robust Underwater Adhesion. *Adv Funct Materials*, **32**(2), 2105464 (2022). https://doi.org/10.1002/adfm.202105464.
69. W. R. Wonderly, T. R. Cristiani, K. C. Cunha, G. D. Degen, J.-E. Shea, J. H. Waite, Dueling Backbones: Comparing Peptoid and Peptide Analogues of a Mussel Adhesive Protein. *Macromolecules*, **53**(16), 6767–6779 (2020). https://doi.org/10.1021/acs.macromol.9b02715.
70. M. A. McCartney *et al*., The Genome of the Zebra Mussel, *Dreissena Polymorpha*: A Resource for Comparative Genomics, Invasion Genetics, and Biocontrol. *G3 Genes|Genomes|Genetics*, **12**(2), jkab423 (2022). https://doi.org/10.1093/g3journal/jkab423.
71. W. Wei, J. Yu, C. Broomell, J. N. Israelachvili, J. H. Waite, Hydrophobic Enhancement of Dopa-Mediated Adhesion in a Mussel Foot Protein. *J. Am. Chem. Soc.*, **135**(1), 377–383 (2013). https://doi.org/10.1021/ja309590f.
72. B. Gabryelczyk *et al*., Hydrogen Bond Guidance and Aromatic Stacking Drive Liquid-Liquid Phase Separation of Intrinsically Disordered Histidine-Rich Peptides. *Nat Commun*, **10**(1), 5465 (2019). https://doi.org/10.1038/s41467-019-13469-8.
73. Y. Sun, Z. W. Lim, Q. Guo, J. Yu, A. Miserez, Liquid–Liquid Phase Separation of Proteins and Peptides Derived from Biological Materials: Discovery, Protein Engineering, and Emerging Applications. *MRS Bull*., **45**(12), 1039–1047 (2020). https://doi.org/10.1557/mrs.2020.301.
74. M. Renner-Rao *et al*., Mussels Fabricate Porous Glues via Multiphase Liquid–Liquid Phase Separation of Multiprotein Condensates. *ACS Nano*, **16**(12), 20877–20890 (2022). https://doi.org/10.1021/acsnano.2c08410.
75. E. Hennebert, B. Leroy, R. Wattiez, P. Ladurner, An Integrated Transcriptomic and Proteomic Analysis of Sea Star Epidermal Secretions Identifies Proteins Involved in

Defense and Adhesion. *Journal of Proteomics*, **128**, 83–91 (2015). https://doi.org/10.1016/j.jprot.2015.07.002.

76. J. N. Israelachvili, P. M. McGuiggan, Adhesion and short-range forces between surfaces. Part I: New apparatus for surface forces measurements. *J. Mater. Res.*, **5**(10), 2223-2231 (1990).
77. E. W. Danner, Y. Kan, M. U. Hammer, J. N. Israelachvili, J. H. Waite, Adhesion of Mussel Foot Protein Mefp-5 to Mica: An Underwater Superglue. *Biochemistry*, **51**(33), 6511–6518 (2012). https://doi.org/10.1021/bi3002538.
78. G. D. Degen, K. C. Cunha, Z. A. Levine, J. H. Waite, J.-E. Shea, Molecular Context of Dopa Influences Adhesion of Mussel-Inspired Peptides. *J. Phys. Chem. B*, **125**(35), 9999–10008 (2021). https://doi.org/10.1021/acs.jpcb.1c05218.
79. G. D. Degen, P. Delparastan, B. D. B. Tiu, P. B. Messersmith, Surface Force Measurements of Mussel-Inspired Pressure-Sensitive Adhesives. *ACS Appl. Mater. Interfaces*, **14**(4), 6212–6220 (2022). https://doi.org/10.1021/acsami.1c22295.
80. G. Violano, G. P. Demelio, L. Afferrante, On the DMT Adhesion Theory: From the First Studies to the Modern Applications in Rough Contacts. *Procedia Structural Integrity*, **12**, 58–70 (2018). https://doi.org/10.1016/j.prostr.2018.11.106.
81. N. Jia, Y. Yao, Z. Peng, S. Chen, Surface Effect in Nanoscale Adhesive Contact. *The Journal of Adhesion*, **97**(4), 380–398 (2021). https://doi.org/10.1080/00218464.2019.1660649.
82. M. Zakeri, J. Faraji, Modeling the Adhesion of Spherical Particles on Rough Surfaces at Nanoscale. *International Journal of Adhesion and Adhesives*, **124**, 103385 (2023). https://doi.org/10.1016/j.ijadhadh.2023.103385.
83. F. L. Leite, P. S. P. Herrmann, Application of Atomic Force Spectroscopy (AFS) to Studies of Adhesion Phenomena: A Review. *Journal of Adhesion Science and Technology*, **19**(3–5), 365–405 (2005). https://doi.org/10.1163/1568561054352667.
84. S. Kim, W. Moon, J. Jeon, A Reliable Method to Measure the Adhesive Force with a Tiny Amount of Adhesive Material. *The Journal of Adhesion*, **84**(1), 60–77 (2008). https://doi.org/10.1080/00218460801888417.
85. K. M. Kimmins, B. D. James, M. T. Nguyen, D. Asker, B. D. Hatton, E. D. Sone, Oil-infused Silicone Prevents Zebra Mussel Adhesion. *ACS Appl. Bio. Mater.*, **2**, 5841–5847 (2019). https://doi.org/10.1021/acsabm.9b00832
86. A. L. Oberg *et al*., Statistical Analysis of Relative Labeled Mass Spectrometry Data from Complex Samples Using ANOVA. *J. Proteome Res.*, **7**(1), 225–233 (2008). https://doi.org/10.1021/pr700734f.
87. M. Mirdita *et al*., ColabFold: Making Protein Folding Accessible to All. *Nat Methods*, **19**(6), 679–682 (2022). https://doi.org/10.1038/s41592-022-01488-1.
88. M. A. Paz *et al*., Specific Detection of Quinoproteins by Redox-Cycling Staining. *Journal of Biological Chemistry*, 266(2), 689–692 (1991). https://doi.org/10.1016/S0021-9258(17)35225-0.

853 *Figures and Tables*

854

855

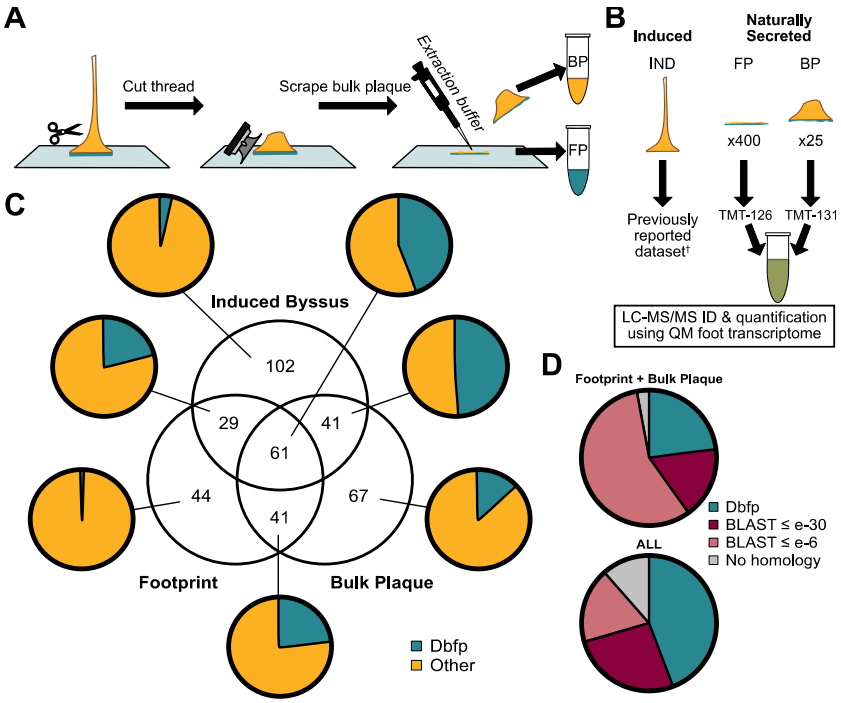

856

857 **Figure 1**: Overview of plaque proteomics investigation. (A) Schematic of sample collection. (B) Summary
858 of workflow. (C) Number of unique proteins found in each group of extractions. Insets indicate the
859 proportion of Dbfp's in each group. (D) Distribution of proteins in the intersecting 'footprint + bulk plaque'
860 group and the 'ALL' group, highlighting the proportion of proteins that are Dbfp's or show strong homology
861 (BLAST score $\leq e^{-30}$), low homology (BLAST score $\leq e^{-6}$), or no homology to known proteins. †(8)

862

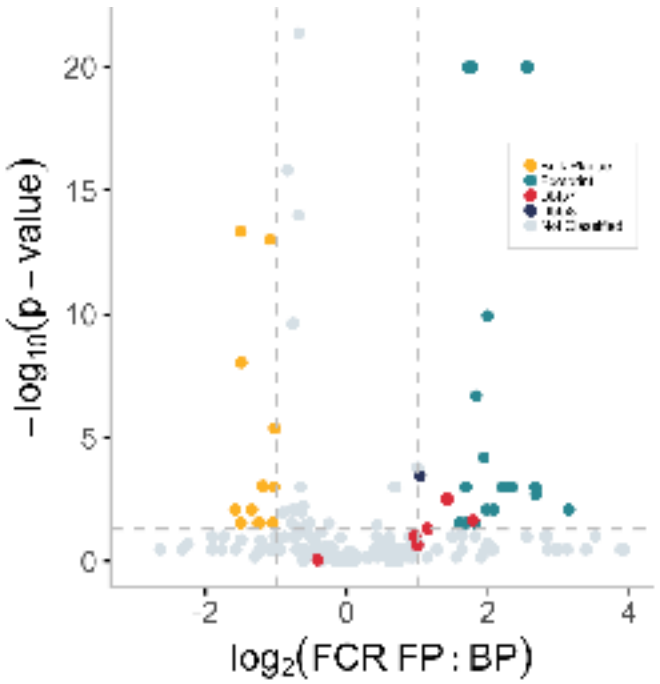

Figure 2: Volcano plot of quagga mussel plaque proteins. Each point represents an identified protein. Proteins with a $\log_2$(fold change ratio between footprint and bulk plaque) > 1 (i.e. > 2 FCR) and a $-\log_{10}$(p-value) > 1.3 (i.e. p-value < 0.05) are significantly enriched in the footprint. Dbfp7 variants and Dbfp8 are indicated as the red and blue points, respectively.

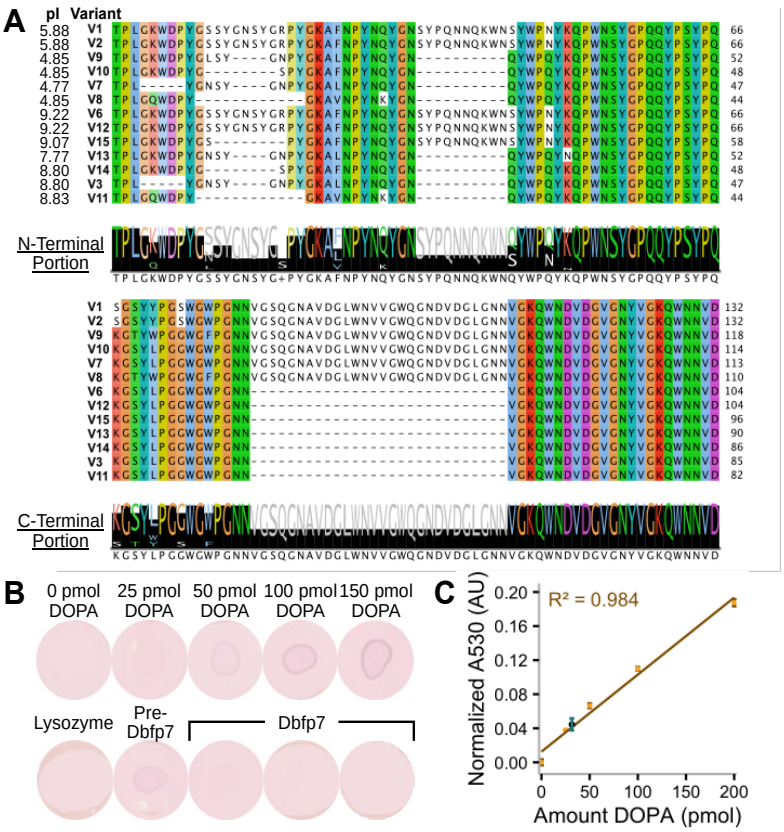

Figure 3: The Dbfp7 protein family is rich in glycine, proline, asparagine, and tyrosine and lacks significant amounts of DOPA. (A) Sequences of Dbfp7 variants. Variants are sorted by length, demonstrating the 28-residue region that is present only in the C-terminal half of the acidic variants. The consensus chart (generated by Jalview 2.11.3.3) below the alignment indicates the residues that are highly conserved, particularly in the C-terminal portion. (B) Dot blot with known amounts of peptidyl DOPA, lysozyme negative control, pre-Dbfp7 HPLC fraction, and Dbfp7 stained with NBT. (C) Calibration curve obtained with known amounts of peptidyl DOPA; the blue point indicates the absorbance of Dbfp7, corresponding to 0.11 ± 0.02 mol% DOPA. Error bars indicate standard deviation (n = 3).

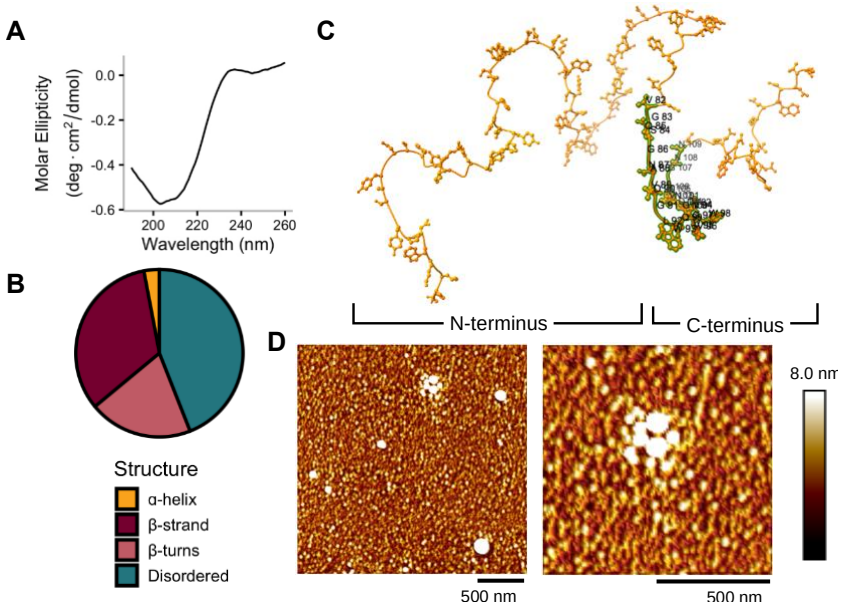

Figure 4: Dbfp7 surface morphology and structure. (A) CD spectrum of Dbfp7 dissolved in 5% acetic acid. (B) Proportion of secondary structure features via deconvolution of CD spectrum by Contin-LL. (C) Predicted structure of Dbfp7 (variant 1) visualized by ChimeraX. Labelled residues indicate the 28-residue C-terminal region found only in acidic variants. (D) Atomic force microscopy height images of Dbfp7 on mica in aqueous conditions. Scalebars each represent 500 nm.

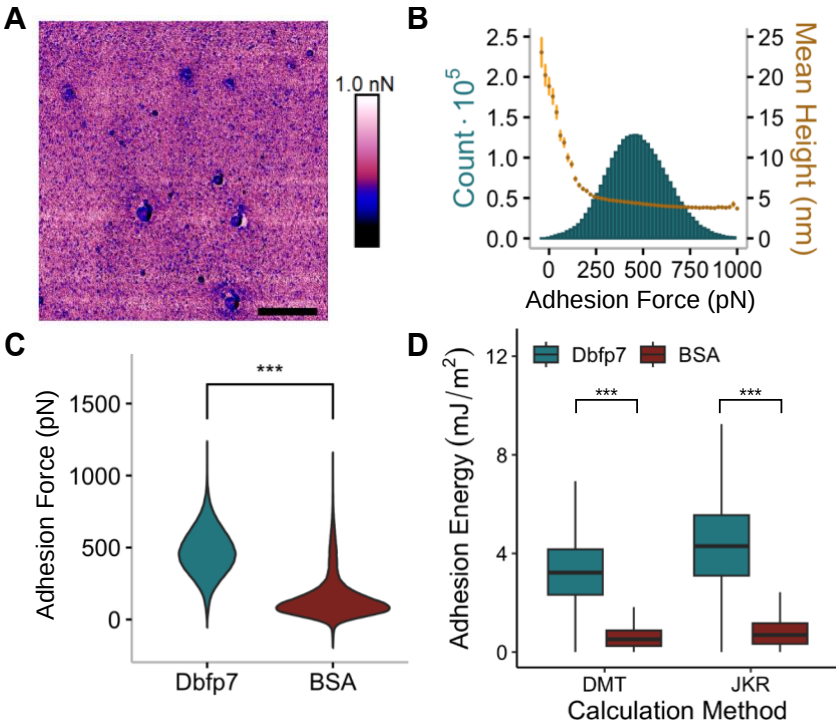

Figure 5: Dbfp7 is adhesive in an aqueous environment. (A) Adhesion map of Dbfp7 (100 µg/mL) coated on mica, imaged in aqueous conditions. Scale bar is 1 µm. (B) The mean height of each bin in the adhesion histogram demonstrates that the areas of low adhesion correspond to regions with taller features. Error bars indicate the standard error of the mean (s.e.m.). (C) Dbfp7 is overall more adhesive than samples prepared with BSA (n = 262,144). (D) Adhesion energy of Dbfp7 and BSA calculated by the DMT and JKR contact models from adhesion force measurements obtained by PFQNM AFM (s.d., N = 2,859,269 and 793,084 for Dbfp7 and BSA, respectively). *** indicates p-value < 0.001.

895 **Table 1**: The quagga mussel footprint proteome in order of relative enrichment in the footprint. Accession
896 #: transcript label and reading frame (0F, 1F, 2F, 0R, 1R, or 2R). $\log_2$(FCR FP:BP): log-transformed fold
897 change ratio between footprint and bulk plaque. $-\log_{10}$(p-value): log-transformed significance value. SP:
898 signal peptide. DOPA: confident (Y), possible (M), or no (N) detection of at least one hydroxylated
899 tyrosine (peptidyl 3,4-dihydroxyphenylalanine) residue via LC-MS/MS sequencing. pI: isoelectric point
900 calculated from the translated transcript sequence. MW: molecular weight calculated from the translated
901 transcript sequence.

Identification	*Accession #*	*$\log_2$(FCR FP:BP)*	*$-\log_{10}$(p-value)*	*SP? (Y/N)*	*DOPA? (Y/M/N)*	*pI*	*MW (kDa)*
Kielin/Chordin-like	comp50443_c0_seq4-0F	3.14	2.10	Y	M	7.99	15.2
Mucin/Spondin-like	comp52859_c0_seq1-1R	2.67	2.70	N	N	4.59	113
Hornerin	comp41116_c0_seq1-2F	2.66	3.00	Y	N	8.06	8.26
Zonadhesin/IgGFc-binding	comp53519_c2_seq1-2R	2.56	20.0	N	M	5.31	125
Zonadhesin/IgGFc-binding	comp53519_c2_seq2-0R	2.53	20.0	N	N	5.25	128
Hornerin	comp36226_c0_seq1-1F	2.33	3.00	Y	N	8.48	16.3
CD109 antigen-like	comp30100_c0_seq2-2F	2.20	3.00	Y	N	4.88	28.2
TPF1III	comp56420_c11_seq1-2F	2.07	2.10	N	N	8.01	8.67
Kielin/Chordin-like	comp31275_c0_seq2-2R	1.99	9.94	N	M	8.16	5.51
TTN1	comp53519_c2_seq3-0R	1.98	2.10	N	N	4.76	35.7
Peroxidase	comp51774_c0_seq1-2F	1.94	4.20	N	N	8.37	83.0
Kielin/Chordin-like	comp31275_c0_seq1-2R	1.82	6.70	Y	M	5.18	13.9
Kielin/Chordin-like	comp30932_c0_seq1-0F	1.81	1.55	N	N	7.53	9.08
Dbfp7	comp52765_c1_seq12-1F	1.79	1.66	Y	Y	9.22	12.0
Fibrillin/Galaxin	comp56544_c0_seq1-2R	1.77	20.0	N	M	5.95	149
Fibrillin/Galaxin	comp56544_c3_seq1-2R	1.71	20.0	N	M	6.91	231
Unknown	comp57807_c0_seq1-0R	1.68	1.55	N	N	8.82	12.4
Galaxin	comp56544_c8_seq1-1R	1.67	3.00	N	N	5.84	29.7
Dbfp7	comp52765_c1_seq11-1F	1.42	2.52	Y	Y	8.83	9.44
Dbfp7	comp52765_c1_seq14-1F	1.14	1.31	Y	Y	8.80	9.90
Dbfp8	comp44862_c1_seq1-2F	1.03	3.45	Y	M	9.99	16.4

902

903